JOURNAL OF PROPULSION AND POWER
Vol. 22, No. 1, January–February 2006

Performance of Supersonic Combustors with Fuel Injection in Diverging Section

Sadatake Tomioka,* Kan Kobayashi,† Kenji Kudo,‡ Atsuo Murakami,‡ and Takeshi Kanda§
Japan Aerospace Exploration Agency, Miyagi 981-1525, Japan

Supersonic combustors with fuel injection in their diverging sections were experimentally tested in a direct-connect wind-tunnel facility at Mach 2.5 and a freestream total temperature of 1500 K. The baseline combustor had backward-facing steps with an expansion ratio of 1.08 at the combustor inlet and a diverging section with a fixed diverging half-angle of 3.1 deg and an expansion ratio of 2.18. Three rows of injectors were installed with an equal streamwise interval within the diverging section. The first half-portion of the diverging section was replaced with one with a diverging half-angle of 1.55 or 6.2 deg and with fuel injector in the cross sections identical to that of second row for the baseline combustor. Room temperature hydrogen was injected at sonic speed through perpendicular orifices, and flow characteristics such as peak pressure rise, expansion pattern, and interaction length were examined. Combustor performances such as combustion efficiency and thrust increment due to fuel injection and combustion were evaluated with a quasi-one-dimensional analysis. Results indicated that fuel injection within the diverging section resulted in a performance as high as that within the upstream constant area section, thus enabling reduction of the length usually required of the isolator section.

Nomenclature

A	=	cross-sectional area of duct
$A(X)$	=	cross-sectional area at X, mm
$\mathrm{d}F$	=	thrust increment
F, F_p, F_r	=	thrust, pressure integration, friction
I_{sp}	=	specific impulse based on thrust increment
p, P	=	pressure
X	=	streamwise location from step
Y, Z	=	spanwise and lateral location from duct center
ε	=	Crocco factor (Ref. 1)
θ	=	half-angle of diverging section
κ	=	specific heat ratio
ϕ	=	equivalence ratio

Subscripts

div	=	diverging section (#1 and #2 for the first- and second-half of the diverging section)
i	=	combustor inlet
inj	=	injection, injector
NF	=	without fuel injection (reference state)
pmax	=	at peak pressure location
w	=	wall
0	=	stagnant condition

Introduction

THE supersonic combustion ramjet (scramjet) engine is a vital part of the rocket-based, combined-cycle engine system for future reusable launch vehicles. One of the most important technologies of the engine operation is suppression of so-called combustor–inlet interaction[1] due to upstream propagation of separation associated with heat release into the inlet section, which causes unfavorable engine unstart conditions. In the tests of a scramjet engine at the Japan Aerospace Exploration Agency–Kakuda Space Propulsion Center[2] (JAXA–KSPC), combustor–inlet interaction occurred and the fuel flow rate was limited below the stoichiometric value.

To mitigate the interaction, a staged supersonic combustor was introduced[3] to suppress the pressure rise in the combustor's minimum cross-sectional area section with marginal sacrifice of thrust, that is, pressure in the following diverging section. A strut with fuel injectors was installed at the minimum section for first-stage injection, and second-stage injectors were installed on the combustor wall within the diverging section. With this staged configuration, a 100% higher thrust increment, that is, an increase in thrust due to fuel injection and combustion, than the first-stage injection alone was obtained.

Installation of struts might cause problems such as severe cooling requirements, structural requirements, and drag production in engine design. Thus, wall injection was employed for both fuel injection stages to eliminate the strut injection.[4] Combustion of second-stage fuel and the consequent pressure rise, however, were quite weak compared to those with the strut/wall staged injection configuration. The second-stage fuel was trapped within the extent of the first-stage fuel, resulting in formation of a fuel-rich region that led to low mixing efficiency. To improve the performance of the combustor with the multistaged wall injection, distributed injections for both the first- and second-staged injections were introduced[5] to stratify the first-stage burnt gas and the fresh freestream and to allow the second-stage fuel to meet the fresh freestream. Whole injection within the diverging section, however, resulted in a larger thrust than that with the distributed multistaged wall injection.

Whereas fuel injection within the diverging section of a supersonic combustor sounds simple, there have been few reports on the performance of a combustor with such an injection scheme. A multi-injection port configuration has been adopted in some engine models, but available data with injection in the diverging section of the combustor are very limited.[6] Vinogradov et al.[7] proposed an engine model with fuel injectors both in the minimum cross-sectional area section and in the diverging section, however, both injectors were used at the same time, making phenomena more complicated.

In the present study, performance of the combustors with fuel injectors within the diverging section was examined experimentally

Presented as Paper 2004-3480 at the AIAA/ASME/SAE/ASEE 40th Joint Propulsion Conference and Exhibit, Ft. Lauderdale, FL, 11–14 July 2004; received 10 February 2005; revision received 29 May 2005; accepted for publication 15 June 2005.

*Senior Researcher, Combined Propulsion Research Group, Kakuda Space Propulsion Center, Kimigaya, Kakuda. Senior Member AIAA.

†Researcher, Combined Propulsion Research Group, Kakuda Space Propulsion Center, Kimigaya, Kakuda. Member AIAA.

‡Senior Researcher, Combined Propulsion Research Group, Kakuda Space Propulsion Center, Kimigaya, Kakuda.

§Senior Researcher, Combined Propulsion Research Group, Kakuda Space Propulsion Center, Kimigaya, Kakuda. Member AIAA.

in a direct-connect wind-tunnel facility. Gaseous hydrogen was injected into a high-enthalpy Mach 2.5 flow through injectors at several streamwise locations within the combustor's diverging section with a typical half-diverging angle of 3.1 deg. A portion of the diverging section was replaced to change the diverging angle. The combustor performance was evaluated based on measured wall pressure distributions and one-dimensionally estimated skin friction and combustion efficiency. Following the performance evaluation, the possibility of performance prediction was pursued by means of the flowfield characterization.

Experimental Apparatus

Wind Tunnel Facility and Test Apparatus

The combustor was directly connected to a blowdown-type wind-tunnel facility with a vitiation air heater to obtain a Mach 2.5 flow with a total temperature of 1500 ± 50 K and a total pressure of 1.0 ± 0.03 MPa. Figure 1 is a schematic of the rectangular combustor and a part of the facility, as well as the coordinate system employed in the present study. The cross-sectional area at the combustor inlet, A_i, was 51 mm in width and 94.3 mm in height. The test section consisted of a constant cross-sectional area isolator section, a constant cross-sectional area combustor section with backward-facing steps (2 mm in height) for flame-holding at its entrance, and a diverging section with a diverging half-angle θ of 3.1 deg (termed the baseline combustor). The cross-sectional area changed from $A/A_i = 1$ to 1.08 at the backward-facing step and from $A/A_i = 1.08$ to 2.35 in the diverging section. Reference 3 contains detailed information on the test facility and the test section. There were four orifices (2.5 mm in diameter) 8 mm downstream of the step on each sidewall for the first-stage wall injection. There were three rows of wall injectors (2.5 mm in diameter, four orifices on each sidewall) installed within the diverging section at streamwise locations of $X = 176$, 296, and 416 mm, the cross-sectional area at injector locations being $A/A_i = 1.33$, 1.59, and 1.84, respectively. Injection configurations with these injector rows were designated as N1, N2, and N3 configurations (N indicates no injection from the first-stage injectors), respectively.

The upstream portion (div.#1 in Fig. 1) of the diverging section ($A/A_i = 1.18 \sim 1.72$) was replaced with a duct with a $q_{\text{div.\#1}}$ of either 1.55 or 6.2 deg. The 3.1-deg diverging portion remained installed for 50 mm at the onset of the diverging section ($A/A_i = 1.08 \sim 1.18$) because of a limitation in the apparatus setup. In each case, fuel injectors were located at streamwise location with its cross-sectional area identical to that of the N2 configuration, $A/A_i = 1.59$, in the baseline combustor, so that both configurations were also designated as N2 configurations. Fuel was also injected from the first-stage wall injector alone, which was designated as the W0 configuration. The configurations are summarized in Table 1. In all cases, room-temperature gaseous hydrogen was injected at sonic speed through perpendicular orifices.

Measurements and Data Reduction

Wall pressure distributions were measured with scanning-type pressure sensors (Scanni valve, with a range of 0–360 kPa and error $\pm 0.25\%$ full scale). The pressure tap intervals for each configuration are summarized in Table 1, the half of the interval being the error for location readings. Wall static pressures were measured along the midheight line of both sidewalls, and pressure distributions shown

Table 1 Injection locations and pressure-tap intervals

		Injector		Extent of pressure tap intervals, mm				
Configuration	$\theta_{\text{div.\#1}}$, deg	X, mm	A/A_i	$\Delta X = 10$	$\Delta X = 5$	$\Delta X = 10$	$\Delta X = 20$	$\Delta X = 40$
W0	3.1	8	1.08	−40∼50 (exp.0), 76∼96		116∼216	216∼336	336∼
N1	3.1	176	1.33	−40∼50 (exp.0), 76∼96		116∼216	216∼336	336∼
N2	3.1	296	1.59	−40∼50 (exp.0), 76∼96		116∼216	216∼336	336∼
N3	3.1	416	1.84	−40∼50 (exp.0), 76∼96		116∼216	216∼336	336∼
N2	1.55	486	1.59	−40∼50 (exp.0), 76∼96		126∼226	226∼346	346∼
N2	6.2	201	1.59	−40∼50 (exp.0), 76∼96	126∼216			251∼

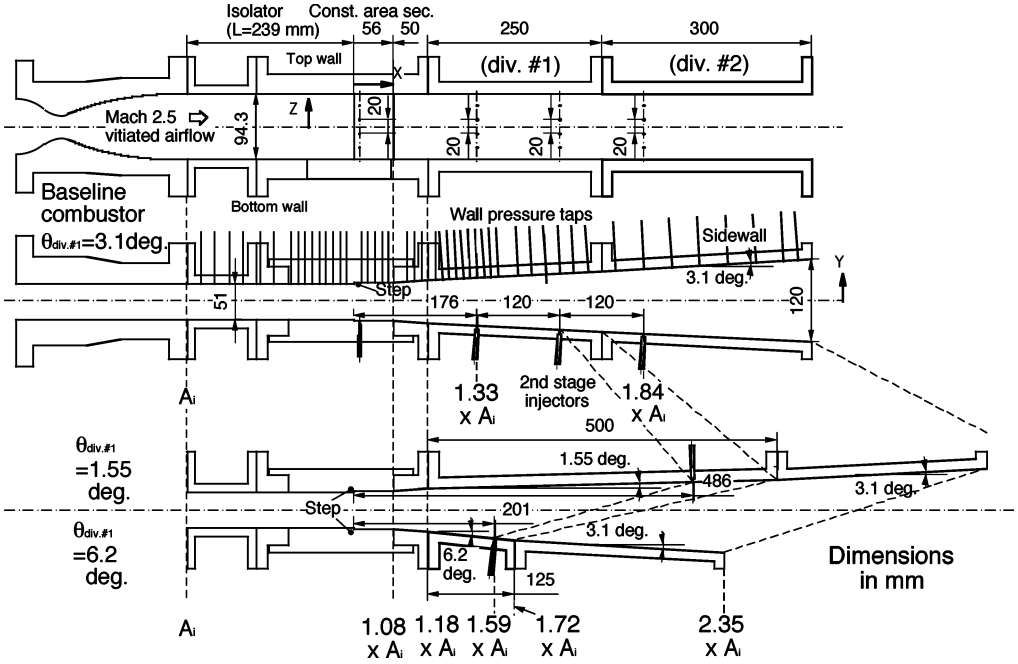

Fig. 1 Schematic diagram of combustor (dimensions in millimeters).

in this paper reflect the average pressures at each axial station. To mitigate the run-to-run deviation of the test conditions, the measured pressure was normalized with the total pressure of the incoming flow, P_0. The repeatability of the nondimensional pressure measurements was within ±5%. In the present study, pressure-rise was defined as local pressure in the case with fuel injection normalized with the value at the same axial station in the case without fuel injection, $p_w/(p_w)_{\mathrm{NF}}$.

Quasi-one-dimensional analysis[3] was used to estimate the flow states as well as skin friction and combustion efficiencies. Skin friction and heat transfer were calculated based on the one-dimensional mean flow states with van Driest method[8] and Reynolds analogy and were taken into account for combustion efficiency calculation. In our previous study,[3] the discrepancy between the one-dimensionally estimated combustion efficiency and the deduced combustion efficiency based on the gas sampling data was 7% at most, being the uncertainty in the one-dimensional combustion efficiency estimation.

The measured wall pressure distribution was integrated to attain the pressure thrust on the combustor, and the skin friction was subtracted to attain the net thrust. The net thrust in the case without fuel injection was subtracted from that in the case with the fuel injection to attain thrust increment, that is, thrust obtained by fuel injection and combustion. During the engine tests at JAXA-KSPC[9] with test conditions close to the current ones, the thrust increment was evaluated based on either the wall pressure integration or a direct measurement of thrust force by a force measuring system. The integrated pressure thrust increment and the directly measured thrust increment agreed well within 5%, showing that the effect of change in friction force due to combustion on the thrust increment was less than 5% of the integrated thrust value. This together with the repeatability in the wall pressure measurement gave the uncertainty in the thrust increment of 10% at most.

One major problem in the analysis was how to calculate the flow state as well as skin friction and heat transfer within a precombustion shock system[1] characterized by flow with separations upstream of the injector locations. In the present study, one-dimensional mean flow states were calculated with mass and momentum conservations and the measured pressure with an assumption that the flow occupied the whole cross section,[1] although the enthalpy conservation was violated.

Experimental Results

Fuel Injection Within the Constant Cross-Sectional Area Section of Baseline Combustor

Initially, the baseline combustor with a constant diverging half-angle of 3.1 deg through the duct was used. In this section, the flowfields without fuel injection and with fuel injection within the constant cross-sectional area section are described.

Figure 2 shows the pressure distributions along the combustor in the case without fuel injection. The variation of the duct cross-sectional area is also shown in Fig. 2. Pressure was almost constant, slightly increasing due to friction, in the constant area section and decreased in the diverging section with a zigzag variation. In the downstream portion of the diverging section, the flow separated from the sidewall because pressure was too low in relation to the atmospheric pressure. In the process of data reduction, a reference distribution without fuel injection was required to estimate the pressure-rise and the thrust increment. However, the measured distribution shown in Fig. 2 was not suitable for use as the reference because of the occurrence of separation at the combustor exit and the zigzag variation. Thus, the pressure distribution between the onset of the diverging section and that of the separation was curve fit with the Crocco equation ($pA^{\varepsilon/(\varepsilon-1)}$, where $\varepsilon = 4.38$ in this case; see Ref. 1) to obtain the reference pressure distribution, shown as a dotted line in Fig. 2.

Also shown in Fig. 2 are the one-dimensionally estimated Mach number and friction coefficient distributions based on the reference distribution mentioned. In the case without fuel injection, only two conservation equations besides the measured static pressure were required to calculate the flow state, and both mass and momentum conservation equations were used[1] in the present study. This calculation method resulted in an error of less than 8% in total temperature at the combustor exit state. The inlet to exit area ratio should yield an exit Mach number of 3.2 for isentropic flow (with typical freestream $\kappa = 1.34$), but reattachment shock wave generation and friction reduced the Mach number at the exit to 2.7.

Figure 3 shows the wall pressure distributions in the case with fuel injection at $X = 8$ mm (the W0 configuration). The fuel equivalence ratio was 0.36. Peak pressure and peak pressure-rise were attained at the fuel injector location. After the peak location, pressure decreased monotonically, even within the constant cross-sectional area section. At the location upstream of the fuel injector, little heat release was expected to take place, whereas the pressure rose monotonically toward the peak value in this portion. Separation due to the adverse pressure gradient associated with heat release penetrated upstream, and the supersonic main flow was compressed before the fuel injection. Kobayashi et al.[10] found that under heat release with a moderate pressure rise the core flow remained supersonic, while the majority of the cross-section was occupied with separation regions. Similar compression of the core flow by a precombustion shock system[1] (PCS) took place in the current condition. With further fuel injection, the separation penetrated the facility nozzle, equivalent to the combustor–inlet interaction in engines of a similar duct geometry.[4]

The one-dimensionally estimated Mach number and combustion efficiency distributions are also shown in Fig. 3. At the location of the peak pressure-rise, the mean Mach number became slightly less than unity, whereas the core flow remained supersonic as already mentioned. The decrease in pressure in the constant area section was, thus, due to the reduction of the separation region toward the end of the section and consequent expansion of the core flow, whereas continuous heat release tended to increase pressure. In the diverging

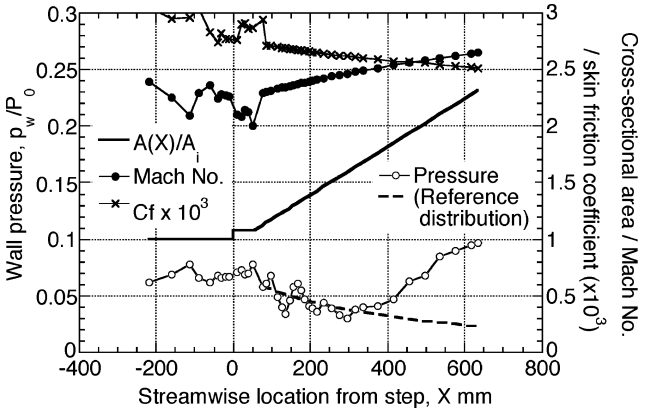

Fig. 2 Wall pressure, one-dimensionally estimated Mach number, and skin-friction coefficient distribution without fuel injection, $\theta_{\mathrm{div.\#1}} = 3.1$ deg.

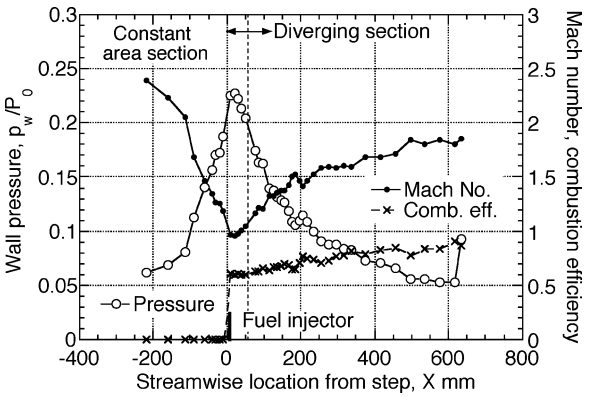

Fig. 3 Wall pressure, one-dimensionally estimated Mach number, and combustion efficiency distributions with fuel injection at $X = 8$ mm, $\theta_{\mathrm{div.\#1}} = 3.1$ deg.

section, pressure decreased monotonically because the expansion overcame the deceleration due to heat release.

Fuel Injections in Different Cross Sections in Fixed-Angle Diverging Section

In this section, the baseline combustor with a constant diverging half-angle of 3.1 deg is described, and the features of the flowfield are examined. Figures 4a–4c show the wall pressure distributions for the N1, N2, and N3 configurations, respectively. With very low fuel flow rates, $\phi < 0.3$, heat release and consequent pressure rise were observed around the separation region at the combustor exit. For the N3 configuration, the same situation was observed with fuel equivalence ratio of up to 0.5. Because these distributions are not of interest here, these data are omitted in the following paragraphs. With an increase in fuel flow rate, the distributions changed in the following manner. First, a peak pressure appeared at locations downstream of the fuel injector showing ignition delay. In this case, the decrease in pressure after the peak location was initially steep and then became moderate, as the reduction of the separation region also occurred within the diverging section. In some cases, another separation occurred at the combustor exit, and these distributions were extrapolated by using the Crocco equation for the one-dimensional calculation. Next, the peak pressure appeared at the injector locations with further fuel flow rate, and the extent of the PCS penetrated farther upstream. The decrease in pressure after the peak location became smoother in these conditions. At fuel flow rates of $\phi > 0.6$, the pressure distributions on both sidewalls were different, the ones with higher peak pressure showing a shorter penetration of the PCS. The distributions on both sidewalls were averaged to attain mean pressure distribution for data reduction in the present study. For the N1 configuration, the PCS penetrated into the constant area section, and even into the isolator, whereas the combustor–inlet interaction was avoided at $\phi \sim 0.9$ because the injector was located farther downstream with a longer distance to the entrance of the isolator section. The PCS for the N2 and N3 configurations was contained within the diverging section up to $\phi \sim 0.9$.

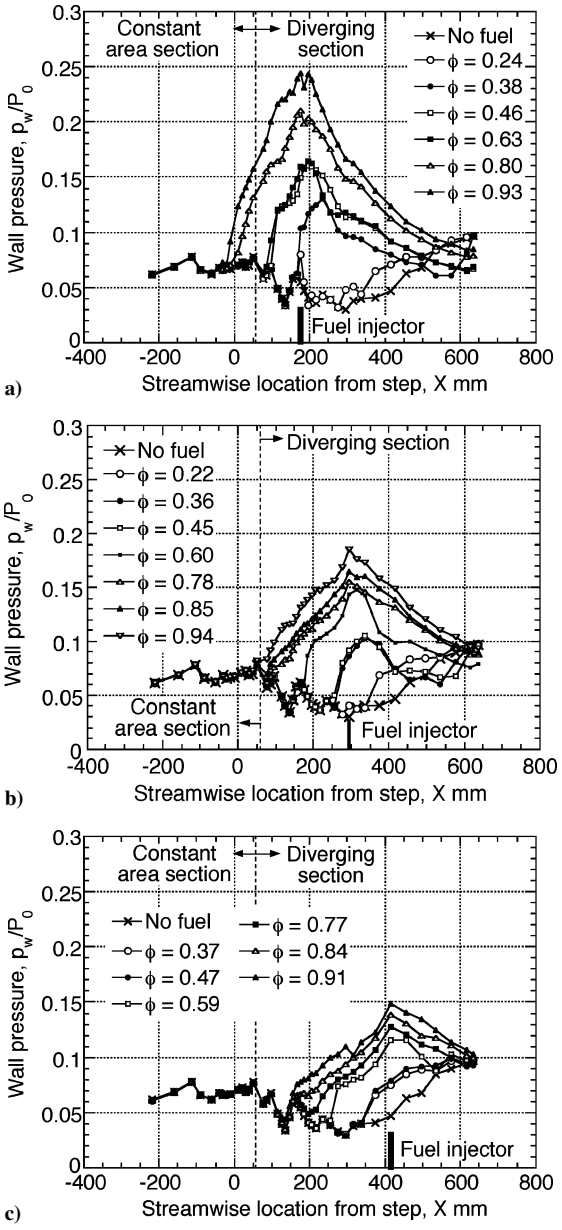

Fig. 4 Wall pressure distributions, $\theta_{\text{div.\#1}} = 3.1$ deg, for a) N1, b) N2, and c) N3 configurations.

Fuel Injection Within the Differently Diverging Sections

In the following section, the diverging half-angle, $\theta_{\text{div.\#1}}$, of the upstream portion of the diverging section was changed to either 1.55 or 6.2 deg, and fuel was injected through the second row of injectors (N2 configuration) at streamwise locations with identical cross-sectional area of $A/A_i = 1.59$ for all diverging angle cases. Note that the diverging half-angle of the downstream portion of the diverging section remained at 3.1 deg. The major objective of introducing the different diverging angles was to determine their effects on the upstream penetration of the pressure rise, so that only the upstream portions with different diverging angles were prepared. However, no sizable pressure rise was observed in the $\theta_{\text{div.\#1}} = 6.2$ deg case with the upstream portion alone, and thus, the baseline downstream portion ($\theta_{\text{div.\#2}} = 3.1$ deg) was attached to sustain combustion by allowing a longer residence time.

Figure 5 shows the pressure distributions along the combustors with the $\theta_{\text{div.\#1}}$ of both 1.55 and 6.2 deg in the case without fuel injection. The variations of the cross-sectional area for each duct configuration are also shown in Fig. 5. In both cases, pressure was identical to that in the baseline combustor within the constant area section and decreased with zigzag variations within the diverging section, until the separation toward the exit occurred. Note that the separation was contained within the downstream portion of the diverging section in both cases. A very steep decrease in pressure was observed at the onset of the $\theta_{\text{div.\#1}} = 6.2$ deg section due to a strong expansion at the onset of this portion. Again, the pressure distributions in the diverging section upstream of the separation region were curve fit with the Crocco equation ($\varepsilon = 2.72$ and 3.55, for the $\theta_{\text{div.\#1}}$ of 1.55 and 6.2 deg, respectively) to obtain reference pressure distributions in both cases, shown as dotted lines in Fig. 5.

Figures 6a and 6b show the pressure distributions in the cases with the $\theta_{\text{div.\#1}}$ of 1.55 and 6.2 deg, respectively, with fuel injection. Unlike the case with the baseline combustor, little difference between the distributions on both sidewalls was found in these cases. In the $\theta_{\text{div.\#1}} = 1.55$ deg case, the peak pressure occurred at the injection location at a fuel flow rate as low as $\phi = 0.35$. There was

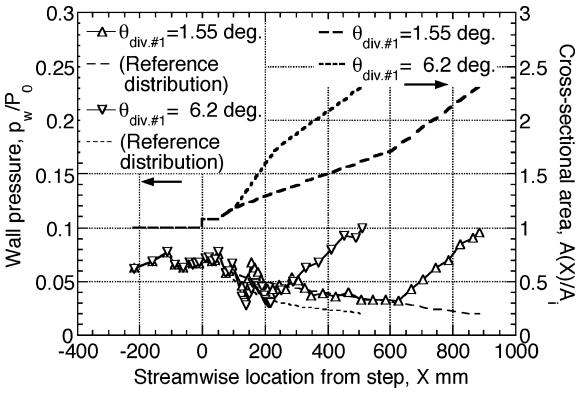

Fig. 5 Wall static pressure distribution without fuel injection at $\theta_{\text{div.\#1}} = 1.55$ and 6.2 deg.

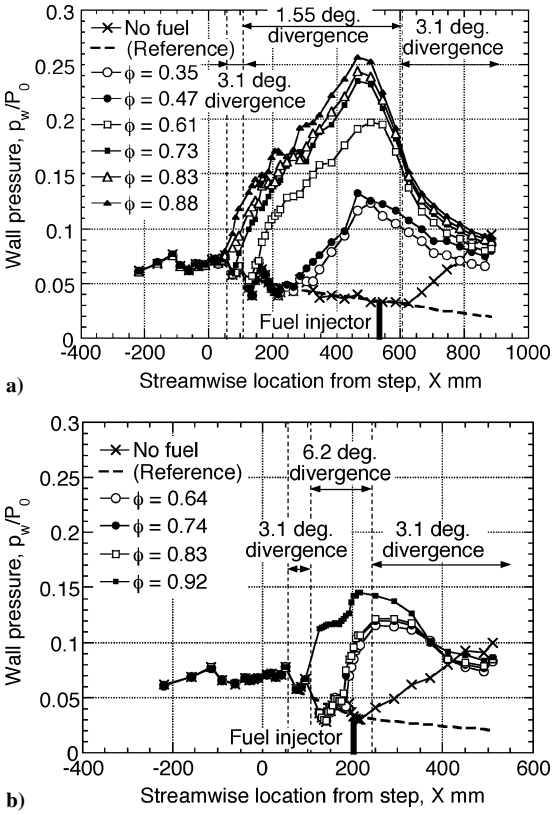

Fig. 6 Wall pressure distributions for N2 configuration at a) $\theta_{\text{div.\#1}}$ = 1.55 deg and b) $\theta_{\text{div.\#1}}$ = 6.2 deg.

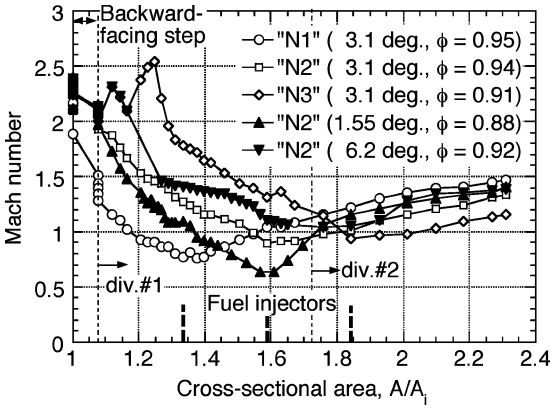

Fig. 7 Comparison of one-dimensionally estimated Mach number distributions with various injection locations or duct configurations at almost identical fuel flow rates, $\phi_2 \sim 0.9$.

a drastic change in the distribution with an increase in fuel flow rate from $\phi = 0.5$ to 0.6, and a steeper decrease in pressure followed by a moderate decrease were observed downstream of the peak location for larger fuel flow rates. This distribution was quite interesting because the downstream portion of the diverging section had a steeper diverging angle; details will be discussed later. In the $\theta_{\text{div.\#1}} = 6.2$ deg case, the peak pressure initially occurred at the junction point between the upstream and downstream portions of the diverging section because oblique shock waves generated by the sudden decrease in diverging angle anchored the flame around the junction point. With the largest fuel flow rate, $\phi \sim 0.9$, the peak pressure occurred at the injector location.

Survey of Flowfield States Estimated with One-Dimensional Analysis

Figure 7 shows a comparison of the one-dimensionally estimated Mach number distributions with various injection locations or duct configurations at almost identical fuel flow rates, $\phi \sim 0.9$. The distributions are plotted against the cross-sectional area.

In the cases with the N2 configuration with $\theta_{\text{div.\#1}} = 1.55$ deg, the mean flow was decelerated to subsonic speed well before the injector location, indicating that even the core flow might decelerate to subsonic speed through a pseudo-shock system.[10] The flow was accelerated to sonic speed around the junction point of the diverging section, so that the flow was choked at that point, and the steep increase in Mach number from the peak location to the junction point was due to heat release causing acceleration of the subsonic flow.

In the cases with the N1 configuration, the mean flow was also decelerated to subsonic speed before the injector location, whereas the flow was accelerated to and beyond sonic speed with neither special geometrical restriction nor steep increase in Mach number. Later discussion will show that the core flow might be still supersonic in this case, showing the difficulty of flow state estimation based on the data measured on the combustor wall.

In other cases, the mean flow was about sonic speed at the injection location, so that the core flow was expected to be supersonic at the injector location, that is, dual-mode scramjet operation was attained. On the other hand, fuel flow rate should be $\phi < 0.6$ to attain the dual-mode scramjet operation for the N2 configuration with $\theta_{\text{div.\#1}} = 1.55$ deg, showing that the duct divergent angle had a sizable effect on the operation-mode control. Note that a pure scramjet operation was attained for smaller fuel flow rate in all cases except for the N2 configuration with $\theta_{\text{div.\#1}} = 1.55$ deg, as shown in Figs. 4. In these cases, the one-dimensionally obtained flow Mach number at the peak pressure location was above unity.

Discussion

Performance Evaluation

In this section, the performances of the combustor, namely, combustion efficiency at the combustor exit and thrust increment within the combustor, are summarized.

Combustion Efficiency

Figure 8 shows a summary of one-dimensionally calculated combustion efficiency at the combustor exit. Combustion efficiency was almost constant or slightly decreased against the fuel flow rate, whereas considerable scatter was observed for the N1 configuration. Thus, the effective equivalence ratio, that is, (equivalence ratio) × (combustion efficiency) indexing heat release, increased with the fuel flow rate. Both a farther downstream injection and a larger diverging angle resulted in a lower combustion efficiency.

Thrust Performance

Figure 9a shows a summary of variations of the thrust increment in combustors against fuel flow rate expressed as equivalence ratios for all cases. Thrust increased with the fuel flow rate in all cases. A farther upstream injection in the baseline combustor and a smaller diverging angle for the N2 configuration both resulted in a higher thrust production in the combustor because combustion efficiency

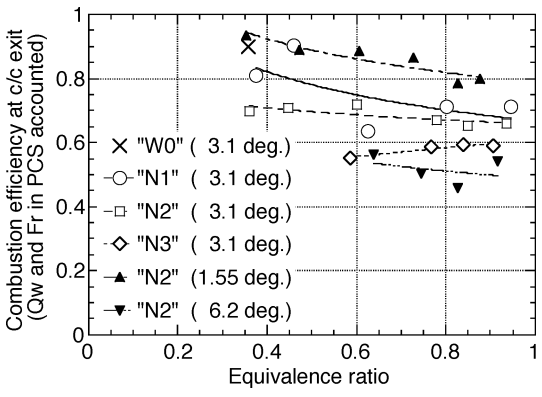

Fig. 8 Summary of one-dimensionally calculated combustion efficiency at combustor exit.

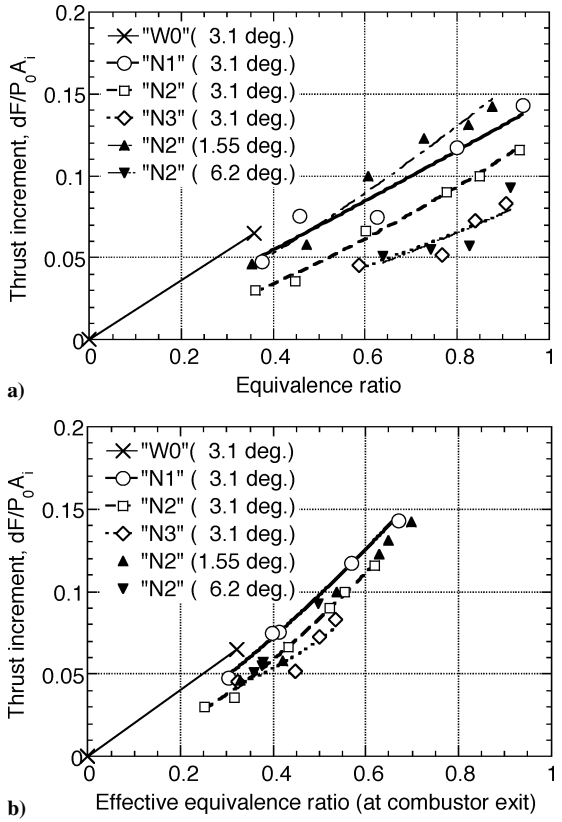

Fig. 9 Variations of thrust increment in combustors against a) fuel flow rate and b) effective equivalence ratio at combustor exit.

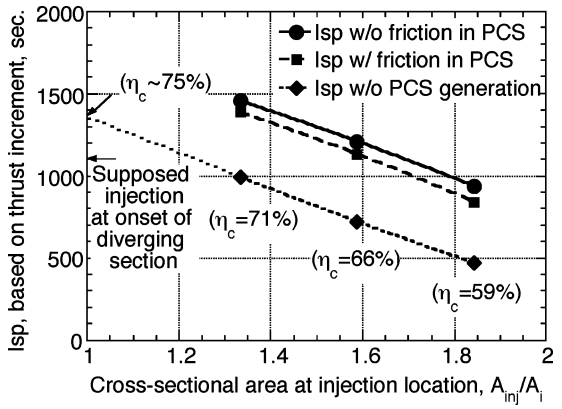

Fig. 10 Effects of PCS generation on combustor performance in case with baseline combustor.

was higher in these cases, as shown in Fig. 8. It was thought that the effects of combustion efficiency on the thrust increment were mitigated if the thrust increments were plotted against the heat release index, that is, the effective equivalence ratio. Thus, in Fig. 9b, the thrust increments shown in Fig. 9a are plotted against the effective equivalence ratio. Nevertheless, a farther upstream injection in the baseline combustor resulted in a larger thrust production, whereas the diverging angle had little effect. These results show that a smaller total pressure loss due to heat release in a lower Mach number flow, that is, in a smaller cross section, was considerably beneficial for thrust production. On the other hand, the lower combustion efficiency for the larger diverging angle was the chief reason for the smaller thrust production in the case with different diverging angles, but this deficiency might be resolved by introducing devices for mixing and reaction augmentation,[11] and the length of the diverging section can be considerably shortened.

Comparison with Case with Conventional Fuel Injection in Constant Area Section

In Figs. 9a and 9b, it can be seen that the conventional fuel injection (the W0 configuration) resulted in a higher thrust performance than the injection in the diverging section (the N$ configurations, where $\$ = 1 \sim 3$) in a lower fuel flow rate regime. In a higher flow rate regime, however, direct comparison between the W0 and N$ configurations was difficult because combustor–inlet interaction occurred in the case with the W0 configuration. Thus, to attain large heat release in the case with the W0 configuration, it is necessary to suppress the separation because the interaction length is quite long in constant area ducts, as will be shown in the following sections. For that purpose, boundary-layer tripping and/or bleeding mechanisms would be useful. In the present study, however, these measures were not available, so that the W0 results were extrapolated from the data with the N$ configurations and are compared with the N$ results in the baseline combustor. Consequently, effects of the PCS generation on combustor performance are also discussed.

The extrapolation method was as follows: First, a PCS generation in the diverging duct produced an extra pressure thrust, which would not be the case for the W0 configuration because the PCS would travel within the constant area duct. Thus, the pressure distribution upstream of the injector location was replaced with the reference distribution, so that the extra pressure thrust obtained by the PCS generation in the N$ cases would be canceled. This case was denoted as the 'without PCS generation' case in the following section because it was equivalent to a suppression of the PCS generation by some means. Next, the thrust datum for each configuration with the baseline combustor at the fuel flow rate of $\phi \sim 0.9$ was plotted against the cross-sectional area at each injector location. The thrust data for the N$ configurations were then extrapolated to attain the performance in the case with injection at the combustor entrance where $A/A_i = 1.0$. The extrapolated W0 datum was now compared with those for the N$ configurations in Fig. 10, showing the combustor performance against the fuel injector location. Note that the thrust increment was normalized with the fuel flow rate to mitigate the deviation in the fuel flow rate. Two cases are shown in Fig. 10, one with the one dimensionally estimated skin friction within the PCS region based on the mean flow condition being accounted for (denoted as the 'with friction in PCS' case) and the other with the skin friction being neglected (denoted as the 'without friction in PCS' case). Because the exact flow states and the corresponding skin friction within the PCS region were not known, actual thrust was thought to lie somewhere between these two values.

First, the effects of the PCS generation on the thrust performance for the N$ cases were examined. The effects are quite evident, delivering a 50%∼100% higher I_{sp}. The extra thrust due to the PCS generation is almost constant regardless of the injector locations, although its fraction to the total thrust is larger with a farther downstream injection. Although the reduction in the skin friction due to the separation resulted in additional extra thrust, its magnitude was 25% or less of the extra pressure thrust production. Note that the extra pressure thrust production due to the PCS generation would be saturated with a farther upstream injection because the PCS region reached the constant area section for the N1 configuration, producing no further extra pressure thrust.

Next, the extrapolated W0 datum was compared with those of the N$ configurations. Because heat release occurred in the lowest Mach number flow, the consequent minimum total pressure loss would lead to the best performance in the extrapolated W0 case. However, this projected best performance can be achieved with injection within the diverging section due to the extra thrust production associated with PCS generation, and these earlier mentioned devices to suppress combustor–inlet interaction are, thus, unnecessary. Furthermore, by containing the PCS within the diverging section, one can reduce the length of the isolator section and, thus, the engine weight. Setting backward-facing steps at the onset of the diverging section would be a good design because the steps were found to anchor the PCS for a certain range of pressure-rise.[12]

Combustion efficiency in each case is noted in Fig. 10, showing the benefit of upstream injection on combustion efficiency. There is

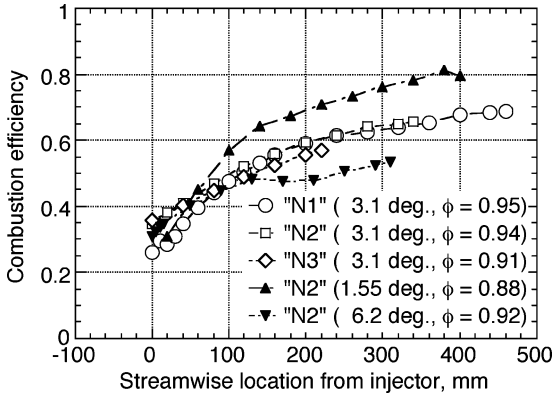

Fig. 11 Comparison of one-dimensionally estimated combustion efficiency distributions against distance from injector location at almost identical fuel flow rates, $\phi \sim 0.9$.

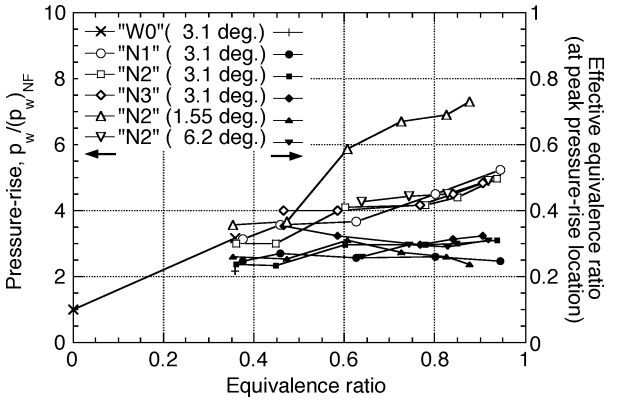

Fig. 12 Peak pressure-rise and one-dimensionally estimated effective equivalence ratio at each peak location.

more room for improvement of performance in the case of injection farther downstream through mixing augmentation.[11]

Flow Characterization Toward Performance Prediction

Inasmuch as the performance of the combustor has been evaluated, the next step is to explore the method of predicting the performance. For conventional combustors, many methods of prediction with simple one-dimensional calculation have been proposed. The simplest is to predict empirically the heat release schedule against the distance from the injector location. Northam and Anderson[13] proposed the mixing schedule as a function of flow geometry and equivalence ratio. Figure 11 shows the one-dimensionally calculated combustion efficiency distributions against the distance from the fuel injector for selective cases, $\phi \sim 0.9$, in the present study. The combustion efficiency distributions agreed with each other for the cases with the baseline combustor (fixed diverging angle), whereas the distributions differed for the cases with different diverging angles, making it difficult to offer general expressions of the heat release schedule.

Another prediction method is to characterize the flowfield (pressure distribution) itself. Mitani et al.[9] showed that a constant Mach number expansion (at $M = 1$) well represented the measured wall pressure distribution within an engine tested under Mach 4 conditions at JAXA–KSPC. Billig[1] used the Crocco equation to predict pressure distributions in supersonic combustors with injection in their minimum cross-sectional area section. This method assumes saturated heat release, that is, $\delta(\text{entropy})/\delta X = 0$, at the combustor exit, which is not suitable for the case with injection farther downstream because the combustion efficiencies were not saturated at the combustor exit in the present study, as shown in Fig. 10.

For performance prediction via characterization of pressure distributions, we should characterize the peak pressure, expansion after the peak location, and penetration of the separation upstream of the peak location. In the following section, data on each topic are characterized as a first step toward establishment of performance prediction methods.

Peak Pressure

The peak pressure value has a very large impact on the thrust production within the combustor. Figure 12 shows a summary of the pressure-rise and the one-dimensionally estimated effective equivalence ratio at each peak location for all cases tested in the present study. The peak pressure-rise increased with the fuel flow rate, this tendency being almost identical in all cases except those in the $\theta_{\text{div.\#1}} = 1.55$ deg case at $\phi \geq 0.6$, that is, under ramjet-mode operation. The datum for the N1 configuration at $\phi \sim 0.9$ was close to those under scramjet-mode operation, implying that the core flow remained supersonic in this case.

The one dimensionally calculated combustion efficiency decreased with the fuel flow rate. However, the consequent effective equivalence ratio at the peak location was almost constant regardless of the fuel flow rate, with an average value of 0.28 and a standard deviation of 0.03. With this value, the peak pressure could be predicted. Note that for the same amount of heat release (and thus, the same total enthalpy), one-dimensional analysis can result in two different flow states, supersonic and subsonic, with a big difference in the pressure level. Thus, this prediction method is only valid for scramjet-mode operation, in which the core flow remains supersonic at the peak location.

Expansion After Peak Pressure Location

Expansion within the diverging section after the peak pressure location plays a key role in the thrust production in the combustor. The pressure variation also reflects the combustion process during the expansion.

To characterize the pressure variations during expansion, the measured pressure distributions (normalized with the peak value) were plotted on a pressure-area (normalized with the area at each peak location) diagram and the Crocco factor ε was calculated for each case by curve fitting the data. The calculated values for all cases in the present study are summarized in Fig. 13a. The obtained values were scattered between 1.5 and 3.5, with an average value of 2.09 and a standard deviation of 0.47. For larger fuel flow rates, $\phi > 0.7$, a farther downstream injection resulted in a larger Crocco factor. In general, however, only a slight tendency was found based on the flow geometry, injection location, and so on. In the next step, the pressure distributions were predicted based on the average Crocco factor, $\varepsilon = 2.09$, and the predicted thrusts in the duct portion after the peak location were compared to the measured value. The deviations of the prediction from the measured values are also shown in Fig. 13a. The deviations were within about $\pm 10\%$, except for the W0 configuration and the N2 configuration with $\theta_{\text{div.\#1}} = 1.55$ deg for $\phi \geq 0.6$, transition to the ramjet mode being the chief reason for the discrepancy in the latter case.

In the next step, the pressure distributions in the diverging section were compared with simpler theoretical ones such as the iso-Mach distributions. In Fig. 13b, the measured pressure distributions for all configurations with fuel injection within the diverging sections at almost identical fuel flow rates, $\phi \sim 0.9$, are plotted on a pressure-area diagram, the values being normalized with values at each peak location. Theoretical distributions expressing an adiabatic expansion after the peak location (typically, $\kappa = 1.27$ for combustion gas) and the $M = 1$ expansion with heat release are shown in the figure. Three distributions expressed by the Crocco equation with $\varepsilon = 1.62$, 2.09, and 2.57 are also presented in Fig. 13 to show the range of the present data at different fuel flow rates. Distribution with a lower Crocco factor was closer to that of the adiabatic expansion, and the measured data for the N2 configuration with $\theta_{\text{div.\#1}} = 1.55$ deg are very close to those of the adiabatic expansion case. There was a relatively long duct with the smaller diverging angle downstream of the injector location in this configuration, allowing a further completion of combustion, as is shown in Fig. 11. Thus, the pressure distribution, especially within the downstream portion of the diverging section, was closer to that for the adiabatic expansion.

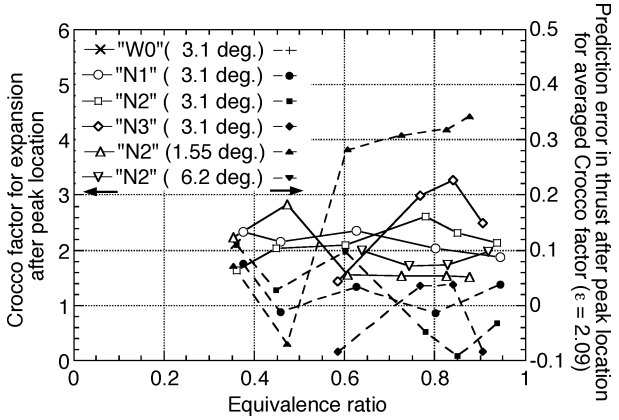

Fig. 13a Summary of Crocco factor for expansion downstream of peak pressure location and thrust prediction error with mean Crocco factor.

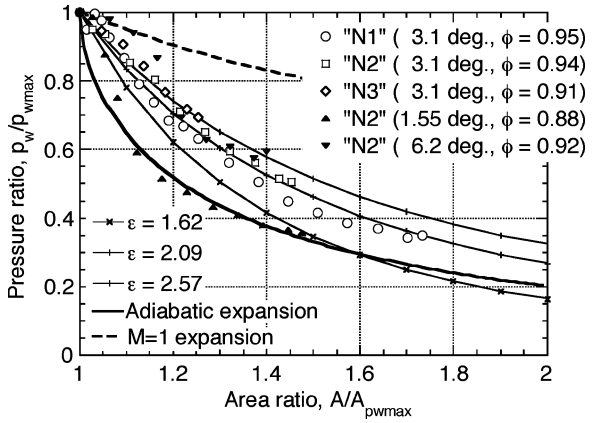

Fig. 13b Variations of pressure against cross-sectional area at downstream portion to each peak location.

Although the pressure distributions for other configurations were expected to be close to that of the iso-Mach expansion as heat release continued in the diverging section, they were intermediate between these two theoretical distributions. Even the distribution with the highest Crocco factor was quite different from the iso-Mach number distribution, indicating that using the iso-Mach number assumption was not appropriate for the present cases.

Penetration of PCS and Thrust Augmentation

In this section, the penetration length of the PCS (interaction length,[1] L_{int}) and thrust augmentation due to the PCS are summarized. Sullins and McLafferty[12] showed that the interaction length to duct height ratio is a function of the pressure-rise in a constant area rectangular duct. Thus, interaction length was normalized with the duct height at the peak location and is shown in Fig. 14a against the peak pressure-rise for each case. The interaction length in a constant area duct expressed by an empirical formula[1,12] is also shown in Fig. 14a; the datum for the W0 configuration is close to the empirical variation. Normalized by the duct height, data for the baseline combustor with different injector locations showed the same variation. On the other hand, data for the N2 configurations with different diverging angles showed that a smaller diverging angle resulted in a longer interaction length, and the data with a smaller diverging angle were closer to those for the case with the constant area duct. The variations with different diverging angles showed a similar tendency, which was quite different from that for the constant area duct. The empirical formula was found to express not only the length but also the pressure distribution within the PCS region.[12] A similar approach is required for the general prediction of the thrust within the PCS region, which is beyond the scope of the present study.

In the present study, as a first step toward general prediction, the gain in thrust due to the PCS generation is summarized in Fig. 14b

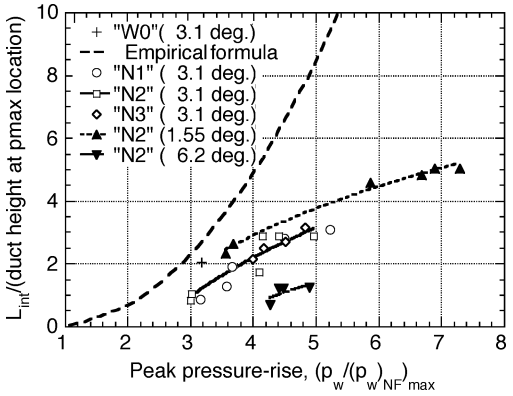

Fig. 14a Interaction length variation against peak pressure-rise.

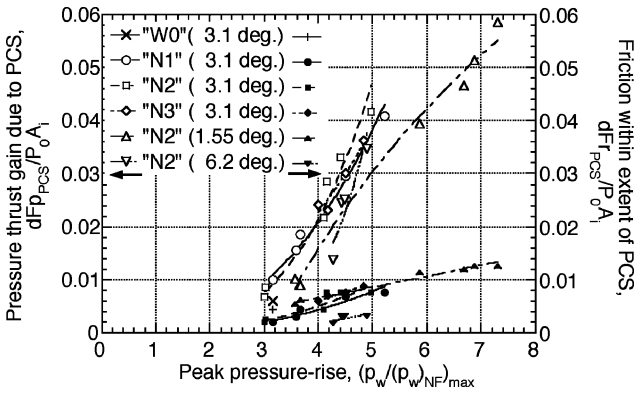

Fig. 14b Gain in thrust with PCS generation against peak pressure-rise.

against the peak pressure-rise predictable in the range of the present condition as mentioned before. The pressure thrust gain was calculated by integrating pressure within the PCS region and by subtracting the freestream value within the PCS region. The friction drag reduction was simply the freestream value within the PCS region because little friction drag was expected within the PCS region. For the same pressure rise, the friction reduction was about a one-quarter of the pressure thrust gain. The variations of the pressure thrust gain for all cases almost fell on a single curve. The variations of the friction reduction also fell on a single curve, except for several deviations (data with $\theta_{\text{div.\#1}} = 6.2$ deg).

Conclusions

The performance of combustors with injection in the diverging section was experimentally investigated in a direct-connect wind-tunnel facility with a combustion heater, which supplied Mach 2.5 airflow with a total temperature of 1500 K. The baseline combustor had a diverging section, $A/A_i = 1.08 \sim 2.35$, with a fixed diverging half-angle of 3.1 deg and three sets of injectors at streamwise locations with cross-sectional areas of $A/A_i = 1.33$, 1.59, and 1.84. A portion of the diverging section, $A/A_i = 1.18 \sim 1.72$, was replaced with one having a diverging half-angle of 1.55 or 6.2 deg, with the injector at a streamwise location with a cross-sectional area of $A/A_i = 1.59$. In all cases, room temperature hydrogen was injected at sonic speed through perpendicular orifices. The following results were obtained.

1) Peak pressure was observed at the injector location for fuel flow rates greater than 0.6 in equivalence ratio, except for the case with the steep diverging angle of 6.2 deg.

2) Combustion efficiency decreased for injection farther downstream and for larger diverging angles of the upstream portion of the diverging section.

3) Combustor performance strongly depended on the injector location, and the separation penetration increased the thrust production by $50 \sim 100\%$.

4) Injection within the diverging section can produce a performance as high as that within the constant area section and can reduce the required length of the isolator section.

5) Peak pressure corresponded to heat release with an effective equivalence ratio of 0.28 ± 0.03, and the expansion after the peak pressure location was expressed with a Crocco factor of 2.09 ± 0.47.

6) Penetration length of the separation upstream of the peak pressure location became greater with the peak pressure-rise values, although the penetration length was smaller compared with that for the straight duct case.

References

[1]Billig, F. S., "Research on Supersonic Combustion," *Journal of Propulsion and Power*, Vol. 9, No. 4, 1993, pp. 499–514.

[2]Kanda, T., Hiraiwa, T., Mitani, T., Tomioka, S., and Chinzei, N., "Mach 6 Testing of a Scramjet Engine Model," *Journal of Propulsion and Power*, Vol. 13, No. 4, 1997, pp. 543–551.

[3]Tomioka, S., Murakami, A., Kudo, K., and Mitani, T., "Combustion Tests of a Staged Supersonic Combustor with a Strut," *Journal of Propulsion and Power*, Vol. 17, No. 2, 2001, pp. 293–300.

[4]Tomioka, S., Kobayashi, K., Kudo, K., Murakami, A., and Mitani, T., "Effects of Injection Configuration on Performance of a Staged Supersonic Combustor," *Journal of Propulsion and Power*, Vol. 19, No. 5, 2003, pp. 876–884.

[5]Tomioka, S., Kobayashi, K., Kudo, K., and Murakami, A., "Distributed Fuel Injection for Performance Improvement of Staged Supersonic Combustor," *Journal of Propulsion and Power*, Vol. 21, No. 4, 2005, pp. 760–762.

[6]Thomas, S. R., and Guy, R. W., "Scramjet Testing from Mach 4 to 20—Present Capability and Needs for the Nineties," AIAA Paper 90-1388, June 1990.

[7]Vinogradov, V., Grachev, V., Petrov, M., and Sheechman, J., "Experimental Investigation of 2-D Dual Mode Scramjet with Hydrogen Fuel at Mach 4. . . 6," AIAA Paper 90-5269, Oct. 1990.

[8]van Driest, E. R., "Turbulent Boundary Layer in Compressible Fluids," *Journal of Aeronautical Sciences*, Vol. 18, No. 3, 1951, pp. 145–160.

[9]Mitani, T., Tomioka, S., Kanda, T., Chinzei, N., and Kouchi, T., "Scramjet Performance Achieved in Engine Tests from M4 to M8 Flight Condition," AIAA Paper 2003-7009, Dec. 2003.

[10]Kobayashi, K., Tomioka, S., Kato, K., Kudo, K., Murakami, A., and Mitani, T., "Performance of a Dual-Mode Combustor with Multi-Staged Fuel Injection," AIAA Paper 2004-3482, July 2004.

[11]Northam, G. B., Stouffer, S. D., Eklund, D. R., and Haimovitch, Y., "Comparison of Wall Mixing Concepts for Scramjet Combustors," International Symposium on Air Breathing Engines, ISABE Paper 95-7108, Sept. 1995.

[12]Sullins, G. A., and McLafferty, G., "Experimental Results of Shock Trains in Rectangular Ducts," AIAA Paper 92-5103, Dec. 1992.

[13]Northam, G. B., and Anderson, G. Y., "Supersonic Combustion Research at Langley," AIAA Paper 86-0159, Jan. 1986.